 CMES, vol.14, no.2, pp.91-100, 2006

A lattice-based cell model for calculating thermal capacity and expansion of single wall carbon nanotubes

Xianwu Ling[1] **and S.N. Atluri**

Abstract: In this paper, a lattice-based cell model is proposed for single wall carbon nanotubes (SWNTs). The finite temperature effect is accounted for via the local harmonic approach. The equilibrium SWNT configurations are obtained by minimizing the Helmholtz free energy with respect to seven primary coordinate variables that are subjected to a chirality constraint. The calculated specific heats agree well with the experimental data, and at low temperature depend on the tube radii with small tubes having much lower values. Our calculated coefficients of thermal expansion (CTEs) are universally positive for all the radial, axial and circumferential directions, and increase with increasing temperature. The armchair tubes see very large circumferential CTEs, while the zigzag tubes see very large axial CTEs. The tube chirality affects mostly the axial and the circumferential CTEs, but not the radial CTEs.

1 Introduction

Carbon nanotubes (CNTs) possess high stiffness and strength and low aspect ratio and density. These extraordinary mechanical properties arouse tremendous interests in CNTs-based nanocomposites [Srivastava & Atluri (2002), Chung & Namburu (2004), Shen & Atluri (2004), Nasdala, Ernst & Lengnick (2005), Gao & Gao (2005)]. Thermal conductance and expansion of the CNTs are two key properties influencing the mechanical behaviors of the nanocomposites in manufacturing and operation. Electrically, a single wall carbon nanotube (SWNT) can be either metallic or semi-conducting depending on its chirality, leading to the possibility to create CNT-based nanoscale electronic device components [Maiti (2002)]. The observation that conductance of a metallic CNT changes by orders in magnitude when strained also opens the door to the potential application of strain-tuned nanoscale electronic transducer, transistor and switcher [Yang, Han & Anantram (2002)]. The thermal properties of CNTs also play critical roles in controlling the performance and stability of these nanoscale electronic components [Liew, Wong & He (2005)].

Many research efforts have been made to determine the specific heat of CNTs, both theoretically and experimentally. Yi, Lu, Zhang, Pan & Xie (1999) experimentally indicated that over the temperature range of $10-300^oK$, the specific heat of multiwall carbon nanotubes (MWNTs) follows a linear temperature dependence, which they attributed to the constant phonon spectrum. Their results indicated that the out-of-plane acoustic mode (as in a graphene sheet) dominated the heat capacity. Mizel, Benedict & Cohen (1999) measured the specific heat for MWNTs in the temperature range $1<T<200^oK$ and found a quadratic temperature dependence of the specific heat at low temperature ($<50^oK$) and a linear temperature dependence above that. Hone, Batlogg, Benes & Johnson (2000) and Popov (2002) made similar observations as Mizel, Benedict & Cohen (1999). Cao, Yan & Xiao (2003) calculated the specific heat using a two-atom unit cell model and the lattice dynamics. The specific heat was found to be proportional to the tubule diameter at low temperatures and inversely proportional to the square of the diameter at high temperatures. Zhang, Xia & Zhao (2003) used a continuum based model to calculate the phonon dispersion relations for SWNTs, based on which they found that the axial lattice wave propagations contributed the most to the specific heat. Li & Chou (2005) calculated the specific heat of SWNTs using molecular structural mechanics and showed that the specific heat increased with increasing tube diameter within the temperature range of $25-350^oK$.

Studies on the thermal expansion of CNTs are very limited. Due to the difficulty in nanoscale experiments, most of the experiments focused on CNT bundles and ropes. Ruoff & Lorents (1995) suggested that the radial coefficient of thermal expansion (CTE) of MWNTs be essentially identical to the axial CTE. The radial CTE

[1] Center for Aerospace Research and Education, University of California at Irvine, 5251 California Ave., Suite 140, Irvine, CA 92612

of MWNTs was found to increase with temperature, nearly identical to that of the c-axis thermal expansion of graphite [Bandow (1997)]. The average tube diameter was observed to increase with increasing growth temperature [Bandow & Asaka (1998)]. Maniwa, Fujiwara, Kira & Tou (2000) reported a radial CTE range of $1.6\times10^{-5}-2.6\times10^{-5}/K$ for the MWNTs. The X-ray studies by Yosida (2000) and Maniwa, Fujiwara & Kira (2001) on SWNT bundles suggested negative radial CTE at low temperatures and positive radial CTE at high temperatures. Although the CTE of SWNT is of fundamental importance to both the nanoelectronics and nanocomposites, experimental data are not available on the CTE for individual SWNT. Theoretical investigations of the thermal expansion of SWNTs are also lacking, and sometimes with contradicting results. Raravikar, Keblinski & Rao (2002) performed MD simulations on $(5,5)$ and $(10,10)$ nanotubes and reported temperature independent positive values for both the radial and axial CTEs. The MD simulations by Kwon, Berber & Tománek (2004) indicated negative CTES for SWNTs up to 900^oK. Jiang & Liu (2004) showed that both the radial and axial CTEs of SWNTs are negative at low temperature but positive at high temperature, but they did not consider the multibody interactions in deriving the atom vibrating frequencies. Lately, the molecular structural approach by Li & Chou (2005) indicated that both the axial and radial CTEs were positive and increase with increasing temperature.

In this paper, we endeavor to analyze the specific heats and the thermal expansion based on a lattice-based cell model. In Section 2, the framework of the cell model for calculating the specific heat and the thermal expansion coefficient is presented. In Section 3, we present results and analysis of the calculated specific heats and CTEs versus temperature and tube radii for different tube chiralities. Section 4 summarizes the work.

2 Cell model for SWNT using the local harmonic approach

The cell model for SWNT is illustrated in Figure 1. In Figure 1, the representative atom A is surrounded by three nearest neighbor atoms B, C and D, forming a lattice cell that can be taken as the basic element of the tube. The second nearest neighbor atoms $B1$, $B2$, $C1$, $C2$, $D1$, $D2$ interact with A through multibody atomistic potentials (e.g., the Tersoff-Brenner potential in below). Now we introduce a polar coordinate system such that $x_A = r$, $y_A = z_A = 0$, where r is the radius of the tube. The polar coordinates of atom B are given by (r, φ_B, z_B), where $\varphi_B = cos^{-1}x_B/r$. The positions of atoms C, D are similarly given. The second nearest neighbor atoms are located using the nearest neighbor atom coordinates. For instance, the equivalence of bond $BB1$ and CA yields

$$\varphi_{B1} = \varphi_B + (\varphi_A - \varphi_C) = \varphi_B - \varphi_C, \tag{1}$$

$$z_{B1} = z_B + (z_A - z_C) = z_B - z_C. \tag{2}$$

Similarly, the positions of B2, C1, C2, D1, D2 can be derived.

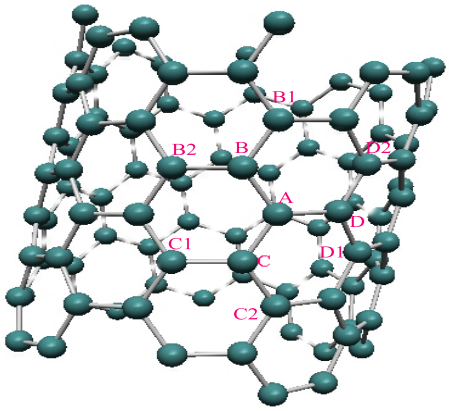

(a) Tubular SWNT

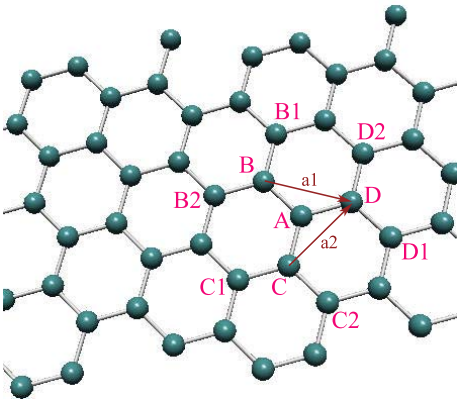

(b) Unrolled planar structure

Figure 1 : Cell model of SWNT in the tubular and unrolled planar structures.

SWNTs can be imagined as a rolled graphene sheet. The unrolled planar graphene sheet, as illustrated in Figure 1(b), can be visualized by cutting the SWNT along its axial direction followed by "unrolling" it *without* stretching

to the tangent plane at A. In the planar graphene, we set a 2D Cartesian coordinate system such that $x_A = 0$, $y_A = 0$. Then, the positions of the nearest neighbor atoms in the 2D Cartesian system are given by $(r\varphi_i, z_i)$, where $i = B, C, D$. The graphene basis vectors $\mathbf{a}_1$ and $\mathbf{a}_2$ are now given by

$$\mathbf{a}_1 = \overrightarrow{BD} = [r(\varphi_D - \varphi_B), z_D - z_B], \tag{3}$$

$$\mathbf{a}_2 = \overrightarrow{CD} = [r(\varphi_D - \varphi_C), z_D - z_C]. \tag{4}$$

In carbon nanotubes (CNTs), the graphene is rolled up in such a way that a graphene lattice vector $\mathbf{c} = n\mathbf{a}_1 + m\mathbf{a}_2$ becomes the circumstance of the tube, where the chirality (n, m) uniquely determines the tube. Utilizing the equations (3) and (4), the circumstance of the tube is now given by

$$\begin{aligned} |\mathbf{c}| &= \sqrt{\mathbf{c}\cdot\mathbf{c}} \\ &= \sqrt{\left(r^2\left[n(\varphi_D - \varphi_B) + m(\varphi_D - \varphi_C)\right]^2\right.} \\ &\quad \left. + \left[n(z_D - z_B) \;\; + m(z_D - z_C) \;\;\right]^2\right). \end{aligned} \tag{5}$$

Meanwhile,

$$|\mathbf{c}| = 2\pi r. \tag{6}$$

Equations (5) and (6) yield

$$\begin{aligned} g = r^2\big(&\left[n(\varphi_D - \varphi_B) + m(\varphi_D - \varphi_C)\right]^2 - 4\pi^2\big) \\ &+ \left[n(z_D - z_B) \;\; + m(z_D - z_C) \;\;\right]^2 \equiv 0, \end{aligned} \tag{7}$$

where g is a geometric constraint that connects the tube chirality to the coordinate variables.

LeSar, Najafabadi & Srolovitz (1989) proposed the local harmonic (LH) approach to calculate the Helmholtz free energy for a finite-temperature equilibrium atomic solid. At the heart of the LH approach is the local description of the atomic vibrations, i.e.,

$$\left|\omega_{i\kappa}^2 \mathbf{I}_{3\times 3} - \frac{1}{m_C}\frac{\partial^2 U_{tot}}{\partial \mathbf{x}_i \partial \mathbf{x}_i}\right| = 0, \quad i = 1, 2, \ldots N, \tag{8}$$

where m_C is the carbon atom mass, U_{tot} is the total potential energy of the system, and ω_i is the vibrating frequencies of atom i (varying from 1 to N – the total number of atoms) in the $\kappa(= 1, 2, 3)$ direction determined with the rest atoms fixed at their equilibrium positions (as implied by the partial derivatives). The LH model neglects the vibration coupling among different atoms, thus providing an computationally efficient and conceptually simple method to calculate the free energy of a system.

In order to calculate the total potential U_{tot}, the interatomic potential is introduced herein. For carbon atoms, we employ the Tersoff-Brenner potential [Brenner (1990)], which is expressed as

$$V_{ij} = V_R(r_{ij}) - \overline{\mathcal{B}}_{ij} V_A(r_{ij}), \tag{9}$$

for atoms i and j, where r_{ij} is the distance between them. The repulsive and attractive terms are given by

$$V_R(r) = \frac{D^{(e)}}{S-1} e^{-\sqrt{2S}\beta(r - R^{(e)})} f_c(r), \tag{10}$$

$$V_A(r) = \frac{D^{(e)} S}{S-1} e^{-\sqrt{2/S}\beta(r - R^{(e)})} f_c(r), \tag{11}$$

where the function f_c is a smooth function used to limit the range of the potential to the nearest neighbor atoms, i.e., $f_c(r) = 1, \frac{1}{2}\{1 + \cos\left[\pi(r - R^{(1)})/(R^{(2)} - R^{(1)})\right]\}, 0$ for $r < R^{(1)}, R^{(1)} < r < R^{(2)}, r > R^{(2)}$, respectively. The parameter $\overline{\mathcal{B}}_{ij}$ takes account of the multibody interaction through the bond angles formed at atom i, and is given by

$$\overline{\mathcal{B}}_{ij} = \frac{1}{2}\left(\mathcal{B}_{ij} + \mathcal{B}_{ji}\right), \tag{12}$$

where

$$\mathcal{B}_{ij} = \left[1 + \sum_{k(\neq i,j)} G\left(\theta_{ijk}\right) f_c(r_{ik}\right]^{-\delta}, \tag{13}$$

$$G(\theta) = a_0\left[1 + \frac{c_0^2}{d_0^2} - \frac{c_0^2}{d_0^2 + (1 + \cos\theta)^2}\right], \tag{14}$$

and where $\cos\theta_{ijk} = r_{ij}^2 + r_{ik}^2 - r_{jk}^2/2r_{ij}r_{ik}$ defines the angle subtended by the adjoint carbon bonds $i - j$ and $i - k$. The material parameters employed in this paper are given in the Appendix.

The Helmholtz free energy using the local harmonic model is now given as [LeSar, Najafabadi & Srolovitz (1989), Foiles (1994)]:

$$H = U_{tot} + k_B T \sum_{i=1}^{N}\sum_{\kappa=1}^{3} \ln\left[2\sinh\left(\frac{h\omega_{i\kappa}}{4k_B T}\right)\right], \tag{15}$$

where k_B and h are the Boltzmann and the Planck's constants, respectively. The total potential U_{tot} directly influenced by a change of atom A's position is reflected in those bonds of the first closest layers, i.e., AB, AC, AD, and through the bond angles in those of the second closet layers, i.e., $BB1, BB1, CC1, CC2, DD1, DD2$. Therefore, the total energy can be expressed as

$$\begin{aligned} U_{tot} &= V_{AB} + V_{AC} + V_{AD} \\ &\quad + V_{BB1} + V_{BB2} + V_{CC1} + V_{CC2} + V_{DD1} + V_{DD2} \\ &\quad + \text{bond energies independent of atom } A. \end{aligned} \tag{16}$$

Jiang & Liu (2004) erroneously neglected the multibody energy contributions represented by the second line on the right-hand side of equation (16), as the second nearest neighbor atoms (*B1, B2, C1, C2, D1, D2*) could not be characterized in their model.

The vibrating frequencies at atom A can now be derived by substituting the total energy U_{tot} (16) into equation (8). In doing so, we point out the seven primary variables (namely, unknowns) in our model, i.e., (φ_B, z_B), (φ_C, z_C), (φ_D, z_D) and r. The second nearest atoms are specified using the bond equivalence as represented by equations (1) and (2). It can be readily proved for a SWNT of a homogenous temperature T, the frequencies $\omega_{i\kappa}$ are independent of the atom i and can be taken the same as those of the representative atom A. However, we need to mention that although the global diagonalization from the quasiharmonic to the local harmonic approaches decouples the vibrating among atoms, the directional coupling within the local harmonic model cannot be readily taken as null. Hence, the off-diagonal component in the local dynamic matrix cannot be neglected as did in Jiang & Huang (2005).

Now the Helmholtz free energy of the system at finite temperature can be obtained as

$$H = U_{tot} + k_B T N \sum_{\kappa=1}^{3} \ln\left[2\sinh\left(\frac{h\omega_{A\kappa}}{4k_B T}\right)\right], \tag{17}$$

where $\omega_{A\kappa}$ is also a function of the primary variables. The total potential energy U_{tot} for the Tersoff-Brenner formalism can be written as

$$U_{tot} = \frac{1}{2}\sum_i \sum_{j\neq i} V_{ij}. \tag{18}$$

Using the bond equivalence, it can be shown that

$$U_{tot} = N U_a, \tag{19}$$

where

$$U_a = \frac{1}{2}\left(V_{AB} + V_{AC} + V_{AD}\right) \tag{20}$$

is the potential energy per atom. Therefore, the Helmholtz free energy per atom H_a for the LH approach can be expressed as

$$H_a = U_a + k_B T \sum_{\kappa=1}^{3} \ln\left[2\sinh\left(\frac{h\omega_{A\kappa}}{4k_b T}\right)\right]. \tag{21}$$

The equilibrium atom positions for SWNTs at homogenous finite temperature T can be obtained by solving for the minimum of H_a, i.e.:

$$\frac{\partial H_a}{\partial \varphi_i} = 0, \quad \frac{\partial H_a}{\partial z_i} = 0, \quad \text{and} \quad \frac{\partial H_a}{\partial r} = 0, \tag{22}$$

where $i = B, C, D$. Note that the minimization is subjected to the nonlinear chirality constraint $g \equiv 0$.

Once the equilibrium configuration is solved, the specific heat per mass is given by [Jiang & Huang (2005)]

$$C_v = \frac{k_B}{m_C}\sum_{\kappa=1}^{3} \frac{\left(\frac{1}{T} - \frac{d\ln\overline{\omega}_{A\kappa}}{dT}\right)\overline{\omega}_{A\kappa}^2}{\sinh^2\left(\overline{\omega}_{A\kappa}\right)}, \tag{23}$$

where

$$\overline{\omega}_{A\kappa} = \frac{h\omega_{A\kappa}}{4\pi k_B T}, \tag{24}$$

is the dimensionless frequency. For numerical convenience, (23) is approximated using a backward difference scheme.

The thermal expansion is characterized by the coefficient of thermal expansion, defined as

$$\alpha_i = \frac{1}{l_i}\frac{dl_i}{dT}, \tag{25}$$

where l_i is the instantaneous length given by

$$l_z = \max\left(z_B - z_C, z_D - z_C\right),$$

$$l_r = r,$$

$$l_c = r\max\left(\varphi_D - \varphi_B, \varphi_D - \varphi_C\right),$$

where z, r, c represent respectively the axial, radial and circumferential directions. In our numerical implementations, a central finite difference scheme is employed to approximate (25), i.e.,

$$\alpha_i = \frac{1}{l_i^T}\frac{l_i^{T+\Delta T} - l_i^{T-\Delta T}}{2\Delta T}. \tag{26}$$

3 Results and discussions

Figure 2 shows the calculated C_v for the armchair (n,n) SWNTs. In Figure 2(a), for comparison purpose, the specific heats for graphite and diamond are also shown. In Figure 2(b), the calculated C_v's are shown for the low temperature range of $2-300^oK$, together with Hone et al. [Hone, Batlogg, Benes, et al. (2000)] measured data for SWNT ropes. Over a wide range of temperature simulated, especially for high temperature above 100^oK, the present analysis agrees well with the experimental data. The results indicate that the specific heats do not depend on the radius of the nanotubes, except at temperature range of $2-300^oK$. This high temperature independence of the specific heat was attributed to the phonon states of the constituent graphene sheet [Hone, Laguno & Biercuk (2002)]. The calculated high temperature specific heats approach the theoretical limit value of $2078mJ/g-K$, regardless of the the chirality and radius of the tube.

Figure 3 shows the specific heats versus the radius of the nanotubes at three levels of temperature. The open symbols represent the data for the armchair tubes, while the the filled tubes represent those for the zigzag tubes $(5,0)$, $(10,0)$, $(20,0)$, $(30,0)$. Figure 3 further confirms that the specific heats are radius independent at high temperature, and that at low temperature, the specific heats show a strong dependence on the tube radius for small tubes and a weak dependence on the tube radius for large tubes. No obvious differences are observed for the armchair and zigzag tubes. We also calculated the C_v for different tube chiralities $(25,m)$, where $m = 0,3,6,9,15,20,25$. Our results (not shown here) indicate that C_v is only very slightly dependent on the chiralities of the tubes and that C_v's for the chirality tubes (with $m = 3,\ldots,20$) are contained in those of the armchair and the zigzag tubes.

Our results deviates below the experimental data for temperature lower than 100^oK. Figure 4 shows the contributions to the specific heat from the three atom vibrating modes for $(10,10)$ tube. As observed by Yi, Lu & Zhang (1999), at low temperature, our results clearly show that the out-of-plane vibrating mode (the radial mode) dominates the specific heat of the SWNT. As the temperature increases, the contributions from the circumferential and then the axial vibrating modes gradually increase. Figure 5 gives the normalized atom vibrating frequencies $\overline{\omega}_\kappa$ for the armchair tubes (n,n). It can be seen that $\overline{\omega}_\kappa$ (expect $\kappa = r$) is quite independent on the radius of the tubes. In Figure 5, we also plot the horizontal line of $\ln(2\sinh\overline{\omega}) = 0$, namely, $\overline{\omega} = 0.48$. Above about 500^oK, $\overline{\omega}_r$ turns to increase, instead of decreasing, the Helmholtz free energy. The radial mode is unique to the SWNTs [Ravavikar, Keblinski & Rao (2002)]. The discrepancy of the calculated C_v at low temperature is caused by the

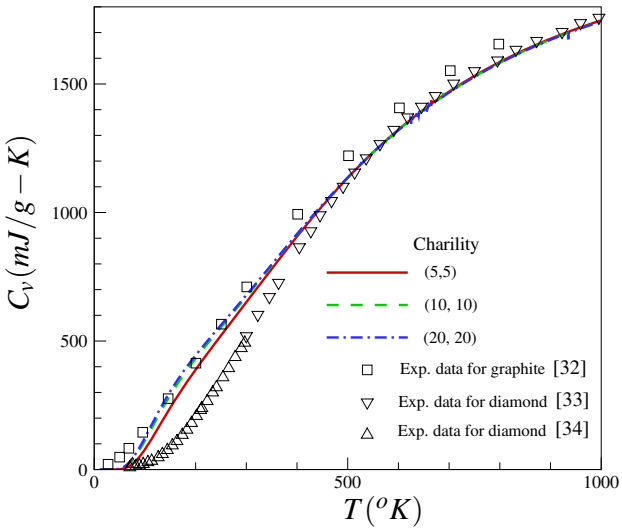

(a) $2-1000K$

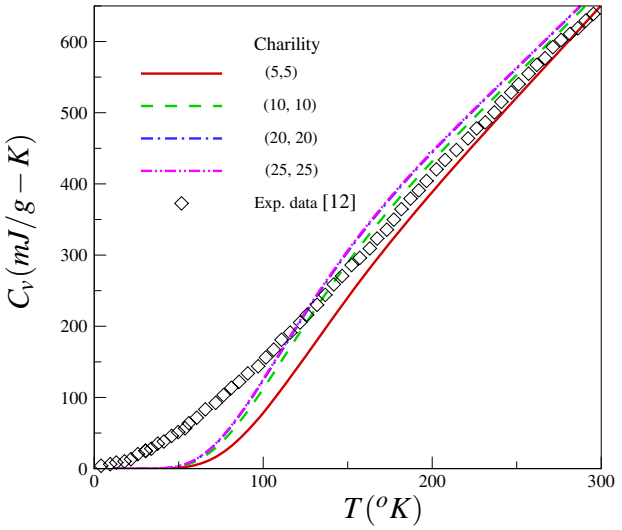

(b) $2-300K$

Figure 2 : Temperature dependence of specific heat for (n,n) SWNTs.

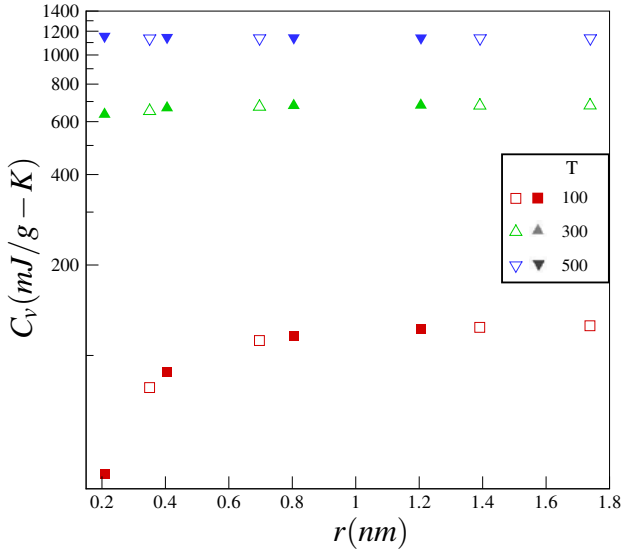

Figure 3 : Radius dependence of specific heats for SWNTs.

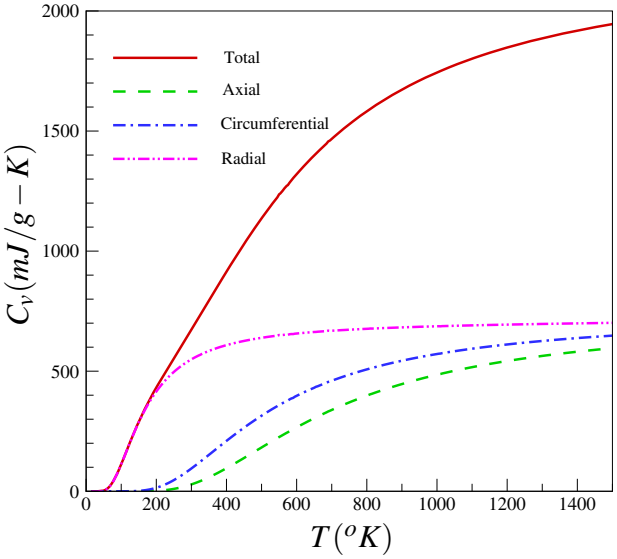

Figure 4 : Mode contributions to specific heats for $(10,10)$ tube.

overestimated radial vibrating frequency, which should be much more constrained by the compressed out-of-plane π bonding orbitals. In the original formalism of Brenner's potential [Brenner (2000)], the π bond is reflected in the multibody term $\overline{\mathcal{B}}_{ij}$ as

$$\overline{\mathcal{B}}_{ij} = \frac{1}{2}\left(\mathcal{B}_{ij} + \mathcal{B}_{ji}\right) + \mathcal{B}^{\pi}_{ij}, \tag{27}$$

where

$$\mathcal{B}^{\pi}_{ij} = \Pi^{RC}_{ij} + \mathcal{B}^{DH}_{ij}, \tag{28}$$

and where the first term Π^{RC}_{ij} represents the influence of radical energetics and π bond conjugation on the bond energies, and the second term $\mathcal{B}^{DH}_{ij}$ depends on the dihedral angle for carbon-carbon double bonds. We tried a constant $\mathcal{B}^{\pi}_{ij} = -0.0243$ (taken from Brenner [Brenner (1990)] for grahpite) in our calculations. The results overpredicted the low temperature specific heat (comparing to the experimental data) by nearly two times, but approached the experimental values at high temperature (starting at $\sim 300^oK$). Due to lack of $\mathcal{B}^{\pi}_{ij}$ data and their derivatives for SWNTs, we made no further attempt in enhancing the calculated low temperature specific heat.

Figure 6 shows the calculated CTE for the armchair, zigzag and chirality tubes. In each case, the axial and circumferential CTEs are also zeroes at 2^oK, but being shifted an amount upwards for clarity. In accordance

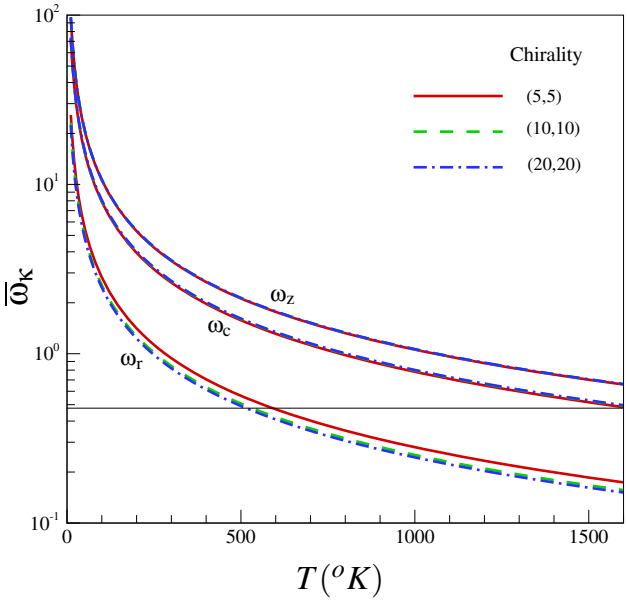

Figure 5 : Normalized atom vibrating frequencies for the armchair tubes.

with Li et al.'s [Li & Chou (2005)] calculations, our results indicate universal positive CTEs for the radial, axial and circumferential directions. As can be seen from 6(a), for the armchair (n,n) tubes, the smaller tubes have slightly higher axial but lower radial CTEs than the larger tubes. The two large tubes $(20,20)$ and $(25,25)$ shows

almost the same CTEs, which means that the CTEs are radius independent for large tubes. To the best the author's knowledge, the circumferential CTE is for the first time reported in the literature. Interestingly, for the armchair tubes, the radial and the circumferential CTEs do not follow the same path. For instance, the small tube $(5,5)$ has a lower α_r but a much higher α_c than those of $(10,10)$, although one might expect $\alpha_c = \alpha_r$. This seemingly contradiction reflects the self-adjusting of the unit cell composed of atoms A, B, C, D in the minimization process of the Helmholtz free energy. For the small tubes, the paradox suggests more self-extension in the circumference.

The CTE variations for the zigzag tubes are shown in Figure 6(b). For the zigzag tubes, the tube radius has a more pronounced effect on the thermal expansion. The large tube $(30,0)$ has a radial CTE that is nearly two to three times larger than that of the small tube $(5,0)$. But the axial CTE for $(30,0)$ is about two to three times lower than that for the small tube $(5,0)$. Very high axial CTEs are observed for the small zigzag tube. Note that the axial direction for the zigzag tubes is the circumferential direction for the armchair tubes. Hence, this observation of high axial CTEs for the zigzag tubes is in accordance with the above observation of high circumferential CTEs for the armchair tube. The explanation for this preference of thermal expansion is simple. Take the armchair tube $(10,10)$ for instance. Table 1 gives the atom positions in the 2D Cartesian system for $T = 300, 1000^oK$. It is seen that atom B moves slightly away from atom A (at $x_A = y_A = 0$) nearly along the circumference, and that C moves slightly away from A nearly along the axial direction. But atom D is also seen to move slightly away along the circumference. Bond AD's circumferential extension, together with bond AB circumferential extension and counterclockwise rotations, causes the large circumferential CTE for the armchair tubes. For the zigzag tubes, no paradox is seen for the circumferential CTEs, which now follows nearly identical paths as the radial CTEs.

Figure 6(c) shows the effect of the chirality on the thermal expansion. Opposite temperature effects are seen for the axial and the radial CTEs. Comparing the armchair and the zigzag tubes, the zigzag tube $(25,0)$ has a much larger axial CTE and a relatively lower radial CTE. And as seen above, the armchair tube has a high circumferential CTE. We need to mention that small local oscillations

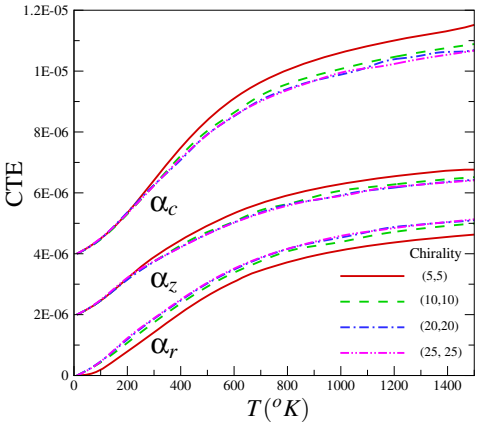

(a) (n,n)

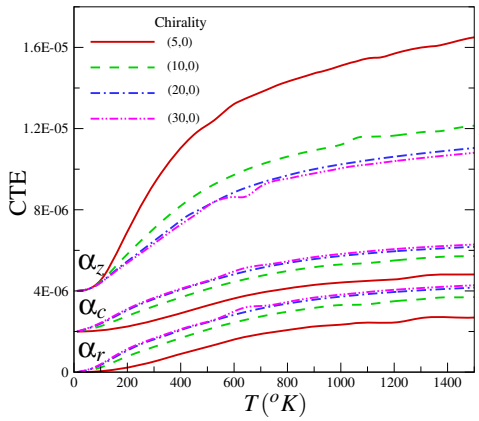

(b) $(n,0)$

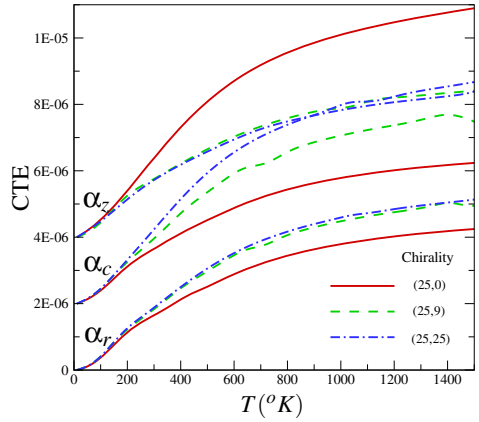

(c) $(25,m)$

Figure 6 : Temperature and chirality dependence of CTEs for SWNTs.

Table 1 : Equilibrium atom positions for $(10,10)$. The length unit is $10^{-2}nm$

.

	B	C	D
300	(-7.294, 12.597)	(-7.267, -12.635)	(14.603, 0)
1000	(-7.330, 12.600)	(-7.264, -12.688)	(14.640, 0)

are seen on the calculated CTEs. This small local oscillations are introduced by the built-in convergence criteria of the IMSL optimizaiton package we used. Small and artificial, they are smoothed out by a polynomial fitting.

4 Summary

In summary, we develop a lattice-based cell model to calculate the specific heats and the coefficients of thermal expansion of single wall carbon nanotubes. The cell model consists of seven primary coordinate variables while subjecting to a chirality constraint.

The specific heat and thermal expansion of the SWNTs are studied. The calculated specific heats are in good agreement with experimental data and for a large range of temperatures, very close to those of graphite and diamond. The chirality dependence of the specific heat is seen only up to a few hundred Kelvins. Small tubes have much lower values at low temperature. Positive thermal expansions are observed for all the radial, axial and circumferential directions. The coefficients of thermal expansion (CTEs) increase with increasing temperatures. For the armchair tubes, both the radial and axial CTEs are only slightly influenced by the tube radii. But the armchair tubes are seen to have large values for the circumferential CTEs. The zigzag tubes have small radial and circumferential CTEs, which also weakly depend on the tube radii. But the zigzag tubes see very large axial CTEs, which also strongly depend on the tube radii. The axial and circumferential CTEs, but not the radial ones, are much influenced by the tube chiralities.

Acknowledgement: This work is supported by the Army Research Laboratory. The first author would also like to thank Dr. Brenner for providing his nanotube code that generates the zero temperature (n,m) carbon nanotubes.

Appendix

The parameters for Brenner's potentials [Brenner (1990)]:

$$D^{(e)} = 6.0eV, \quad S = 1.22, \quad \beta = 21nm^{-1},$$
$$R^{(1)} = 0.17nm, \quad R^{(2)} = 0.27nm, \quad R^{(e)} = 0.139nm,$$
$$a_0 = 0.00020813, \quad c_0 = 330, \quad d_0 = 3.5.$$

The carbon bond length for the zero temperature graphene sheet is set to $0.14507nm$. The other constants are given as: $m_c = 1.9926 \times 10^{-26}Kg$. The Planck's constant $h = 6.626068 \times 10^{-34}Js$. And the Boltzmann constant $k_B = 1.3806503 \times 10^{-23}JK^{-1}$.

References

Allen, M.; Tildesley, D. (1987): *Computer Simulation of Liquids*. Oxford University Press.

Srivastava D., Atluri S.N. (2002): Computational Nanotechnology: A current perspective, *CMES: Computer Modeling in Engineering & Science*, vol. 3, pp. 531-538.

Chung P.W., Namburu R.R., Henz B.J. (2004): A Lattice Statics-Based Tangent-Stiffness Finite Element Method, *CMES: Computer Modeling in Engineering & Science*, Vol. 5, pp. 45-62.

Shen S.P., Atluri S.N. (2004): Computational Nanomechanics and Multi-scale Simulation, *CMC: Computers, Materials & Continua*, vol. 1, pp. 59-90.

Nasdala L., Ernst G., Lengnick M. & Rothert H. (2005): Finite Element Analysis of Carbon Nanotubes with Stone-Wales Defects, *CMES: Computer Modeling in Engineering & Science*, Vol.7, pp. 293-304.

Guo W.-L. and Gao H.-J. (2005): Optimized Bearing and Interlayer Friction in Multiwalled Carbon Nanotubes, *CMES: Computer Modeling in Engineering & Science*, Vol. 7, pp. 19-34

Maiti A. (2002): Select applications of carbon nanotubes: field-emission devices and electromechanical sensors, *CMES: Computer Modeling in Engineering & Science*, vol. 3, pp. 589-599.

Yang L., Han., Anantram M.P. (2002): Bonding geometry and bandgap changes of carbon nanotubes under uniaxial and torsional strain, *CMES: Computer Modeling in Engineering & Science*, vol. 3, pp. 675-685.

Liew K.M., Wong, C.H., He X.Q., & Tan T.J. (2005): Thermal stability of single and multi-walled carbon nanotubes, *Phys. Rev. B*, vol. 71, 075424.

Yi W., Lu L., Zhang D.L., Pan Z.W., & Xie S.S (1999): Linear specific heat of carbon nanotubes, *Phys. Rev. B*, vol. 59, 9015.

Mizel A., Benedict L.X., Cohen M.L., et al. (1999): Analysis of the low-temperature specific heat of multiwalled carbon nanotubes and carbon nanotube ropes, *Phys. Rev. B*, vol. 60, 3264?270.

Hone J., Batlogg B., Benes Z., Johnson A.T., Fischer J.E. (2000): Quantized phonon spectrum of single-wall carbon nanotubes, *Science*, vol. 289, pp. 1730-1733.

Popov V.N. (2002): Low-temperature specific heat of nanotube systems, *Phys. Rev. B*, vol. 66, 153408.

Cao J.X., Yan X.H., Xiao Y. (2003): Specific heat of single-walled carbon nanotubes: a lattice dynamics study, *J. Physical Society of Japan*, vol. 72, 2256-2259.

Zhang S.L., Xia M.G. & Zhao S.M. (2003): Specific heat of single-walled carbon nanotubes, *Phys. Rev. B*, vol. 68, 075415.

Li C.Y., Chou T.W. (2005): Quantized molecular structural mechanics modeling for studying the specific heat of single-walled carbon nanotubes, *Phys. Rev. B*, vol. 71, 075409.

Ruoff R.S., & Lorents D.C. (1995): Mechanical and thermal properties of carbon nanotubes, *Carbon*, vol. 33, pp. 925?30.

Bandow S. (1997): Radial thermal expansion of purified multiwall carbon nanotubes Measured by X-ray diffraction, *Jpn. J. Appl. Phys.*, vol 36, pp. L1403-L1405.

Bandow S., & Asaka S. (1998): Effect of the growth temperature on the diameter distribution and chirality of Single-Wall Carbon Nanotubes, *Phys. Rev. Letters*, vol. 80, pp. 3779-3782.

Maniwa Y., Fujiwara R., Kira H., & Tou H. (2000): Multiwalled carbon nanotubes grown in hydrogen atmosphere: An x-ray diffraction study, *Phys. Rev. B*, vol. 64, 073105.

Yosida Y. (2000): High-temperature shrinkage of single-walled carbon nanotube bundles up to 1600 K, *Journal of Applied Physics*, vol. 87, pp. 3338-3341.

Maniwa Y., Fujiwara R., Kira H., & Tou H. (2001): Thermal expansion of single-walled carbon nanotube (SWNT) bundles: X-ray diffraction studies, *Phys. Rev. B*, vol. 64, 241402 (R).

Raravikar N.R., Keblinski P., & Rao A.M. (2002): Temperature dependence of radial breathing mode Raman frequency of single-walled carbon nanotubes , *Phys. Rev. B*, vol. 66, 235424.

Kwon Y.-K., Berber S., & Tománek (2004): Thermal Contraction of Carbon Fullerenes and Nanotubes, *Phys. Rev. Letters*, vol. 92, 015901.

Jiang H., Liu B., et al. (2004): Thermal expansion of single wall carbon nanotubes, *J. Engng. Mater. Tech.*, v126, pp. 265-270.

Li C.Y., Chou T.-W. (2005): Axial and radial thermal expansion of single-walled carbon nanotubes , *Phys. Rev. B*, vol. 71, 235414.

LeSar R., Najafabadi R., Srolovitz D.J. (1989): Finite-temperature defect properties from free-energy minimization, *Phys. Rev. Letters*, vol. 63, pp. 624-627.

Brenner D.W. (1990): Empirical potential for hydrocarbons for use in simulating the chemical vapor deposition of diamond films, *Phys. Rev. B*, vol. 42, pp. 9458?471.

Foiles S.M. (1994): Evaluaiton of harmonic methods for calculating the free energy of defects in solids, *Phys. Rev. B*, vol. 49, 14930.

Jiang H., et al. (2005): A finite temperature continuum theory based on interatomic potentials, *Trans. of the ASME*, vol. 127, pp. 408-416.

Hone J., Laguno M.C., Biercuk M.J., et al. (2002): Thermal properties of carbon nanotubes and nanotube-based materials, *Appl. Phys. A*, vol. 74, pp. 339-343.

Madelung L.-B., et al. (1982): Physics of Group IV elements and III-V compounds, New series, Group III, vol. 17, Springer-Verlad, Berlin.

Billings B.H., & Gray D.E. (1972): American Institute of Physics Handbook, McGraw-Hill, New York.

Pitzer K.S. (1938): The heat capacity of diamond from 70 to 300^{o}K, *Journal of Chemical Physics*, vol. 6, pp. 68-70.

Ravavikar N.R., Keblinski P., Rao A.M. (2002): Temperature dependence of radial breathing mode Raman frequency of single-walled carbon nanotubes, *Phys. Rev. B*, vol. 66, 235424.

Brenner D.W. (2000): The art and science of an analytic potential, *Phys. Stat. Sol. (b)*, vol. 217, pp. 23-40.